Sunspike Detection Using Radial-by-Radial Noise Estimates

Brandon Taylor*

CIMMS - NWS Radar Operations Center - Norman, Oklahoma

**Corresponding author address:* Brandon Taylor, Radar Operations Center, 1424 Halley Ave., Norman, Oklahoma, 73069.

E-mail: Brandon.M.Taylor@noaa.gov

ABSTRACT

Sunspikes, or the incidental intersection of the radar receive path with the sun's radio emissions, are an integral part of the core methods used by the Radar Operations Center to calibrate the Differential Reflectivity of the WSR-88D fleet. A method had been developed within the Radar Operations Center for post processing the Level II data to find instances of these sunspikes. This method relied on using the sun's geophysically referenced position in tandem with the derived SNR from reflectivity values to determine if a direct sunspike was observed. After the release of Software Build 14.0 and attendant introduction of Radial-by-Radial Noise Estimation, this method became untenable. Sun noise censors the sunspike reflectivity signature, as it raises the noise floor at the sunspike radial. As such, Radial-by-Radial noise estimates replaced the derived SNR estimates from reflectivity within the algorithm. This led to the introduction of unwanted weak sunspike instances, which were invariant in elevation, as compared with results the previous reflectivity method yielded. This paper explains how the algorithm was corrected, and the extra data pared. A proxy for SNR was found. This proxy was the ratio of the peak sunspike noise to the legacy Blue-Sky noise, which was used as the global noise value before Radial-by-Radial noise was introduced. It has been shown that this ratio is representative of SNR, and it can be used to filter the data. Henceforth, this ratio will be referred to as SPNR (Sunspike Noise Ratio or Spike Noise Ratio).

1. Introduction

Sunspikes are named as such due to the “spike” in the received power throughout the radials where the sun’s radio emissions were encountered. These occurences have proved useful in regards to the efforts of many to externally measure antenna pointing bias, as established in Muth et al. (2012), Reimann (2013), and Holleman et al. (2010b). Ice et al. (2014) discusses how the Radar Operations Center engineering team has taken advantage of these to improve engineering calibration practices. More specifically, the sun can be used to calibrate differential reflectivity, while at the same time monitoring the pointing bias of the antenna. This is possible due to the sun’s intrinsic differential reflectivity of zero, as presented by Holleman et al. (2010a) and Zrnic et al. (2006). Fig. 1 shows how the differential reflectivity tend towards zero near the origin of the pointing chart. Using the sun as a baseline for calibration is a passive method which requires no extra equipment or expenditure; the only requirement is identifying and processing the sunspikes in the operational radar datasets. The operational reflectivity signature of a sunspike is represented on a Plan Position Indicator (PPI) display as a strobe which fills all bins down a radial with power. During calibration procedures where the sun is tracked by the radar, called solar box scans, the signature of the sun appears more intuitively as a circular disk, seen in Fig. 2. Previously, sunspikes were detected and assimilated through the method developed by Cunningham et al. (2013). The original algorithm for detecting sunspikes considered all bins in a radial to determine admission into the usable set of sunspikes to create a composite pointing plot. The signal-to-noise ratio (SNR) was calculated at each bin, and the number of bins between 10-15 dB were summed, which ensured that the sunspike was in fact direct, and that weather did not contaminate the results. Radial-by-Radial (RxR) Noise Estimation was introduced in Build 14 by the Radar Operations Center in mid-2014. Ivić et al. (2013) describes how the algorithm dynamically estimates the system noise power from in-phase and quadrature data components. With the radially specific estimates, the power received from the sun essentially censors itself by raising the calculated noise floor, as seen in Fig. 3. The algorithm was no longer able to detect sunspikes due to loss of the reflectivity strobes. Fig. 4b demonstrates how the new method was detrimental to the pointing estimates as compared to the original in Fig. 4a. Revisions to the algorithm were made in order to resolve the undesirable sun hit distribution; these changes are discussed here.

2. Method

Two techniques for measuring the solar image are presented here. The first, which was used in the original sunspike detection method, relies on reflectivity to calculate SNR values. The second method, which is the new method, uses noise power to calculate the Sunspike Noise Ratio (SPNR) values. The Sunspike Noise Ratio, or Spike Noise Ratio, is a new term coined to describe the ratio of a sunspike's peak RxR noise value with the noise floor. Here, the noise floor used is the 'Blue-Sky' Noise, as discussed by Free and Patel (2005). Griffiths and Libert (1994) use a ratio similar to SPNR, comparing the noise output of the system with the antenna pointed at the sun to that when the antenna is pointed at the 'cold-sky'. Their application was the evaluation of an antenna's gain-to-noise-temperature ratio. Using MATLAB to read and process Level II data, it is shown that SNR and SPNR are nearly equivalent, and the advantages and disadvantages of using the second method as compared to the first are discussed.

a. Sunspike Algorithm Review

The sunspike detection algorithm has number of criteria to filter for sunspikes. It restricts the assimilation of radar datasets to those from Volume Coverage Pattern (VCP) 31 and 32 (clear-air mode), in order to avoid precipitation contamination. Because of considerations for atmospheric refraction, elevation angles of 1.5 degrees are used for VCP 32 and 2.5 degrees for VCP 31. These cuts are known as the surveillance cuts, used to determine long range reflectivity, apropos for detecting sunspikes. Table 1 gives an overview of all the parameters which filter for sunspikes.

b. Measuring the Solar Image using Reflectivity

The original sunspike algorithm measured the strength of the sunspike by summing the number of bins down a radial which had an SNR at or between 10 dB and 15 dB. This is incompatible for comparison with RxR Noise, as only one noise value is produced per radial. In order to get a single value from the radial, a method for determining the received solar power at the antenna feed is required. In order to determine this power, the calibration of reflectivity signals by the signal processor must be undone by removing the range dependence, atmospheric attenuation, and the radar constant. Eq. A1 from Huuskonen et al. (2014) with amendments achieves this, where r is range (km), a is the one-way gaseous attenuation (dB km^{-1}), and C_r is the radar constant. The median of all the powers at each bin down a radial is then taken to arrive at a single value per radial. The original equation considered spectral power, whereas this analysis requires only power. Fig. 5 compares the two methods, showing that they yield very similar values for SNR and SPNR. The datasets comparing the methods come from the same cuts, but RxR noise was turned on in one and off in the other, achieved through simulated playback of Level I data through the RDA. Yet, because of the simplistic statistics used to arrive at a single value per radial, the relation breaks down at lower SNRs. A more sophisticated approach that yields values which better match SPNR is shown in Fig. 11. With this approach, a distribution of SNR in relation to elevation is obtained in Fig. 9 that matches the original constraints in the algorithm of values between 10-15 dB.

c. Measuring the Solar Image using Noise Power

The Radial-by-Radial Noise algorithm estimates the system noise power in real time. Radial-by Radial Noise measurements are taken at each antenna pointing position, and output directly to the Level II data. Fig. 6 depicts this perspective of a sunspike. In order to achieve this, the algorithm searches the radial for flat sections in the power profile, or areas where there is no weather, and uses these areas as a proxy for noise. When a sunspike is encountered by the radar, the power profile becomes noisy and devoid of flat sections. Fig. 7 demonstrates that with a sunspike power profile full of signal the noise estimates are raised, as there are no sections devoid of signal. Although the sun's radio emissions are highly incoherent according to Dulk (1985), they are sampled as coherent by the signal processor. The algorithm essentially measures the received power from the sun, i.e. the power is leaking into the noise estimate. Finding the ratio of the RxR noise value down the sunspike radial with the Blue-Sky noise, essentially yields the SNR. Fig. 8 depicts the quadratic dependence of SPNR on radar elevation angle. After including the 10 dB SPNR threshold, which has been shown as a characteristic value of SNR for sunspikes from research on the KOUN radar by Zrnic et al. (2006), it is shown that the distribution of SPNR with elevation in Fig. 9 is very similiar to the distribution of SNR with elevation, as shown in Fig. 10.

3. Results and Discussion

Fig. 13 shows how the use of a thresholding value in the algorithm corrects the invariance in elevation.

Azimuthal precision is increased through the new RxR sunspike detection, as seen in the decrease of the angular width of the solar image as measured by RxR noise compared with that measured by reflectivity. According to astronomical measurements of solar radio emission by Kundu (1965), the angular distance to the sun center should be around 0.5°, as demonstrated in Fig. 12. From Fig. 13 it is seen that the elevation width is accurately portrayed, but the azimuth is somewhat constrained, reaching out to around 0.3°. This may be due to the convolution created by the scanning motion of the antenna, but it is most likely that the RxR noise method for detecting sunspikes increases the precision in choosing the correct radial.

4. Conclusions

a. Considerations on the Algorithm

It was impossible to test the new algorithm's ability to detect sunspikes before RxR noise estimation became operational in 2014, as it takes a month or more of sun hits to create pointing estimates needed to validate it. There was no existing theory on using RxR noise, so this explains why original logic in the new algorithm was faulty.

b. Advantages of RxR Sunspike Detection

There are many advantages to using RxR noise for sunspike detection and validation. Since it is a measure of noise and not power, it can distinguish between weather and a sunspike, unlike SNR. In the future, the ROC may be able to incorporate more than just clear-air VCPs into the algorithm. With other VCPs included, this will also introduce sunspikes at various elevations. Furthermore, the new algorithm is not capped at 15 dB, which allows for the admission of the most direct sunspikes. This could greatly improve differential reflectivity calibration efforts, as near-perfect point hits have the most chance of measuring the sun's actual intrinsic differential reflectivity of zero.

Acknowledgments. Many thanks to Rich Ice for being a continual support throughout this project and providing me with all of his reference texts from his personal library. Jane Krause also provided input into the project, and I couldn't have done this project without the Level II data playback with Radial-by-Radial noise off and on that she provided. Lindsey Richardson was a great help with MATLAB nuances.

References

Cunningham, J. G., W. D. Zittel, R. R. Lee, R. L. Ice, and N. P. Hoban, 2013: Methods for Identifying Systematic Differential Reflectivity (ZDR) Biases on the Operational WSR-88D Network. *36th Conference on Radar Meteorology*.

Dulk, G. A., 1985: Radio emission from the sun and stars. *Annual review of astronomy and astrophysics*, **23**, 169–224.

Free, A. D., and N. Patel, 2005: Clutter censoring theory and application for the WSR-88D. *32nd Conference on Radar Meteorology*.

Griffiths, H., and M. Libert, 1994: Assessment of a technique for measurement of antenna g/t using solar noise. *Novel Antenna Measurement Techniques, IEE Colloquium on*, IET, 6–1.

Holleman, I., A. Huuskonen, R. Gill, and P. Tabary, 2010a: Operational monitoring of radar differential reflectivity using the sun. *Journal of Atmospheric and Oceanic Technology*, **27 (5)**, 881–887.

Holleman, I., A. Huuskonen, M. Kurri, and H. Beekhuis, 2010b: Operational monitoring of weather radar receiving chain using the sun. *Journal of Atmospheric and Oceanic Technology*, **27 (1)**, 159–166.

Huuskonen, A., M. Kurri, H. Hohti, H. Beekhuis, H. Leijnse, and I. Holleman, 2014: Radar performance monitoring using the angular width of the solar image. *Journal of Atmospheric and Oceanic Technology*, **31 (8)**, 1704–1712.

Ice, R. L., A. Heck, J. Cunningham, and W. D. Zittel, 2014: Challenges of polarimetric weather radar calibration. *8th European Conference on Radar and Hydrometeorology*.

Ivić, I. R., C. Curtis, and S. M. Torres, 2013: Radial-based noise power estimation for weather radars. *Journal of Atmospheric and Oceanic Technology*, **30 (12)**, 2737–2753.

Kundu, M. R., 1965: Solar radio astronomy. *New York: Interscience Publication, 1965*, **1**.

Muth, X., M. Schneebeli, and A. Berne, 2012: A sun-tracking method to improve the pointing accuracy of weather radar. *Atmospheric Measurement Techniques*, **5 (3)**, 547–555.

Reimann, J., 2013: On fast, polarimetric non-reciprocal calibration and multipolarization measurements on weather radars. *Qucosa*.

Zrnic, D. S., V. M. Melnikov, and J. K. Carter, 2006: Calibrating differential reflectivity on the wsr-88d. *Journal of Atmospheric and Oceanic Technology*, **23 (7)**, 944–951.

APPENDIX

A1. Abbreviations

RxR: *Radial-by-Radial*

PPI: *Plan Position Indicator*

SNR: *Signal-to-Noise Ratio*

SPNR: *Sunspike Noise Ratio or Spike Noise Ratio*

ROC: *Radar Operations Center*

VCP: *Volume Coverage Pattern*

KMHX: *Morehead City, NC Radar site*

KLSX: *St. Louis, MO Radar site*

KOUN: *Research Radar located at Max Westheimer Airport/OU North Research Campus*

KABR: *Aberdeen, SD Radar site*

WSR-88D: *Weather Surveillance Radar 1988 Doppler*

Build 14: *Software Build released by the ROC which dictates the operations of the WSR-88D network*

MATLAB: *Matrix Laboratory, a software program used for data analysis and processing*

RDA: *Radar Data Acquisition*

A2. Additional Figures and Tables

LIST OF TABLES

TABLE 1: Governing parameters of the Original Sunspike Algorithm from Cunningham (2013)

Parameter	*Filter*
VCP	31, 32
Elevations	1.5°, 2.5° (surveillance cut)
Range	20 to 460 km
Signal-to-Noise Ratio	$>$ 10 dB and $<$ 15 dB
Bin Count	$>$ 1000
Volume Scans	3 closest to target elevations, sunrise and sunset
Radial	Best positional matching

LIST OF FIGURES

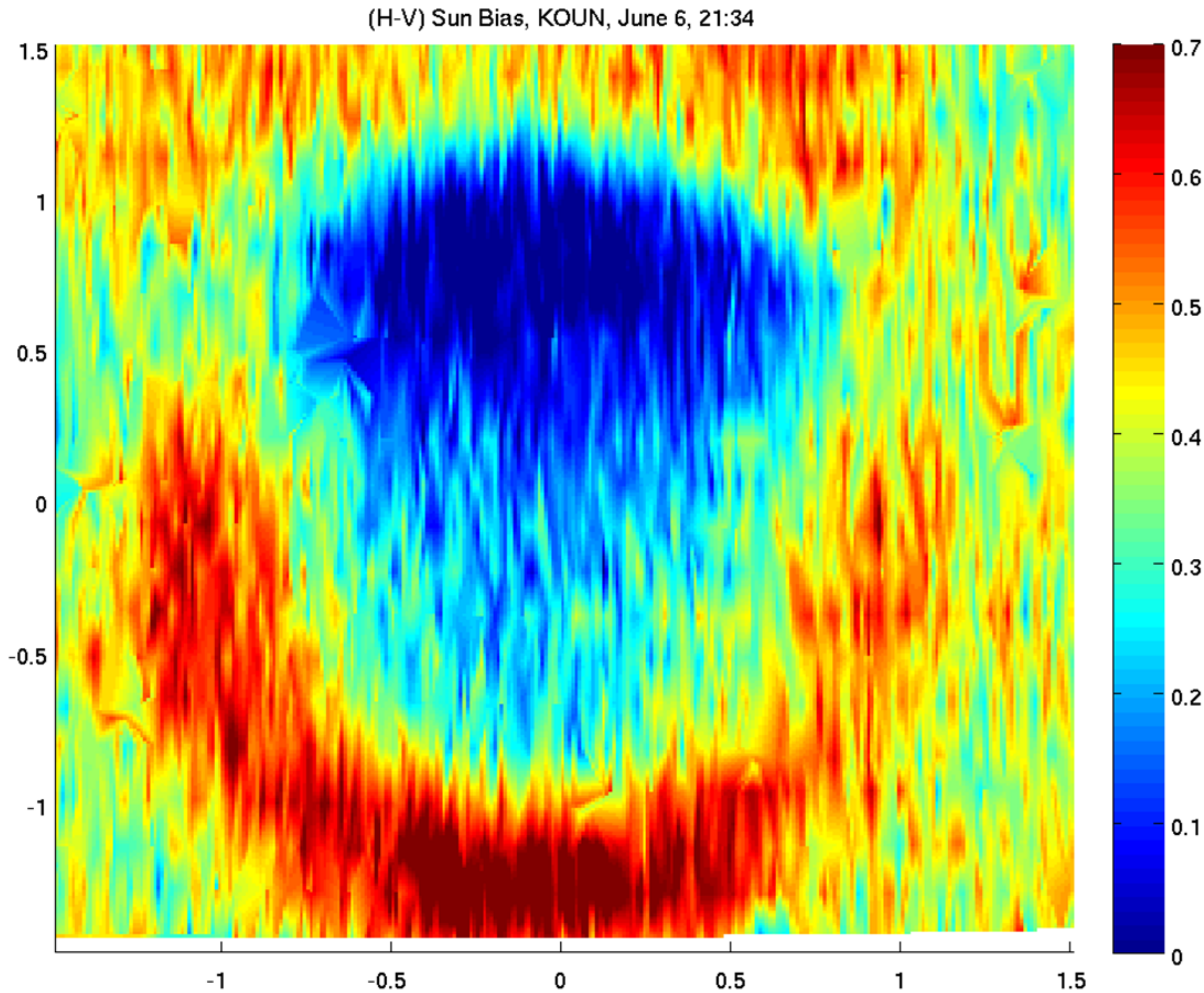

FIG. 1: Z_{DR} representation of the solar image. Colorfill is Z_{DR} in dB.

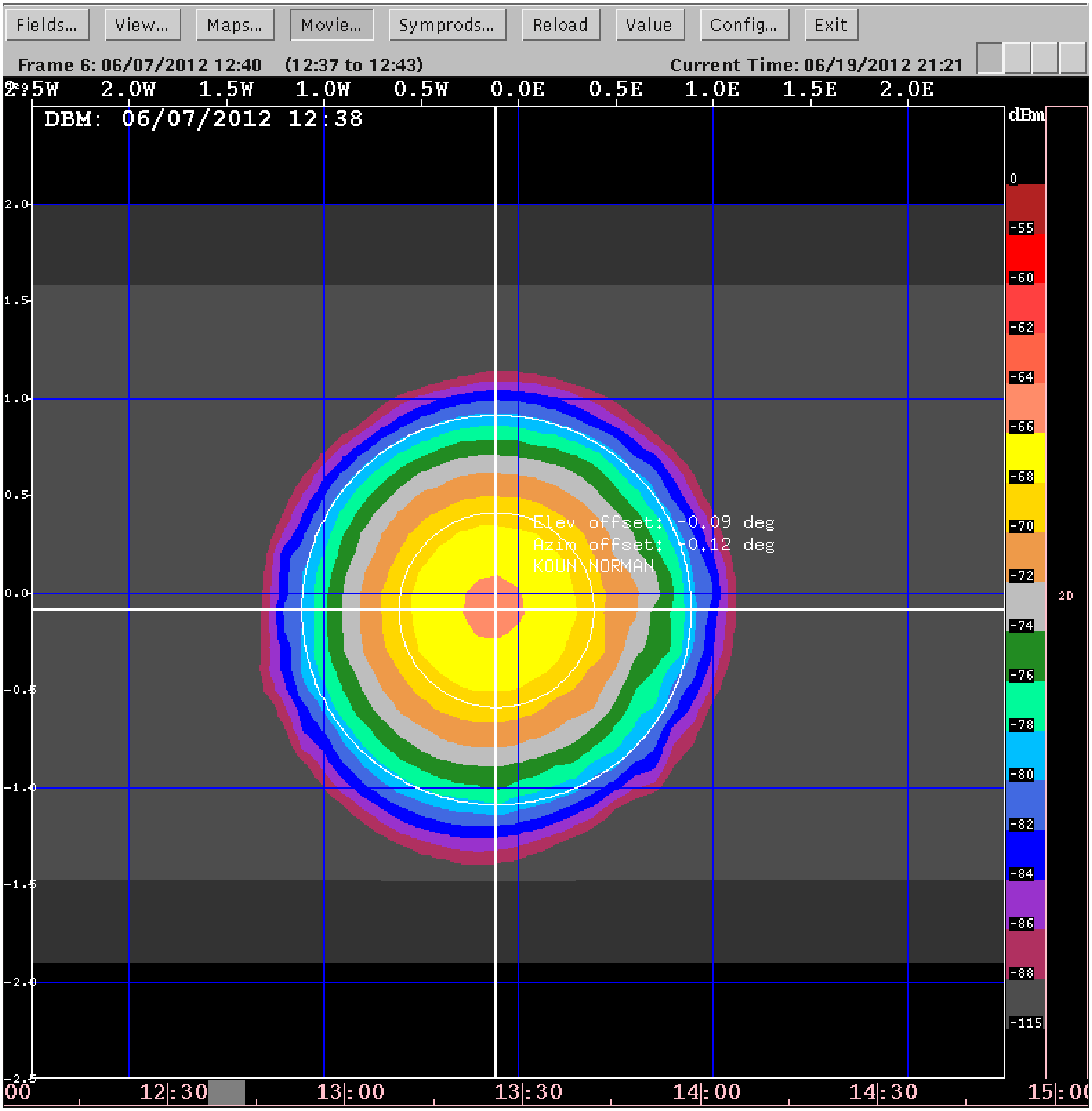

FIG. 2: Power representation of the solar image taken at KOUN. Colorfill is power in dBm.

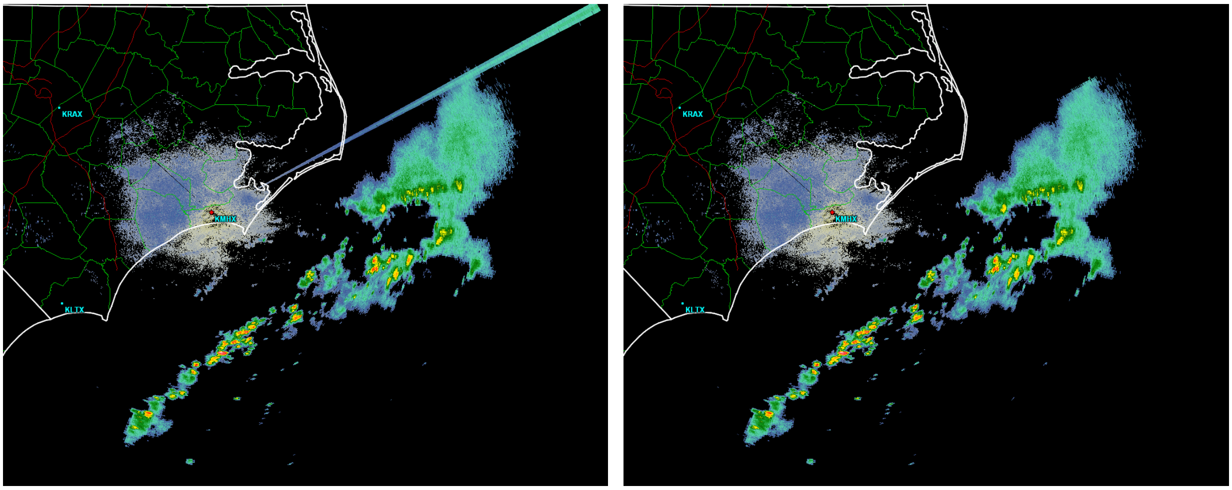

(a) RxR noise off

(b) RxR noise on

FIG. 3: Comparing the reflectivity of sunspikes with RxR noise off and on.

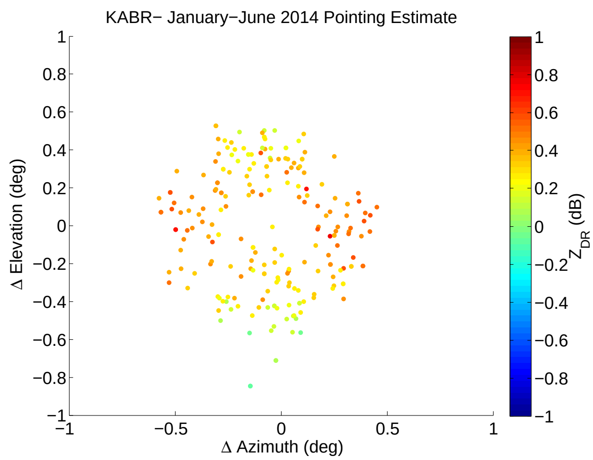

(a) A sun image collected at the KABR radar from January-June 2014. The color fill indicates the median Z_{DR} in dB.

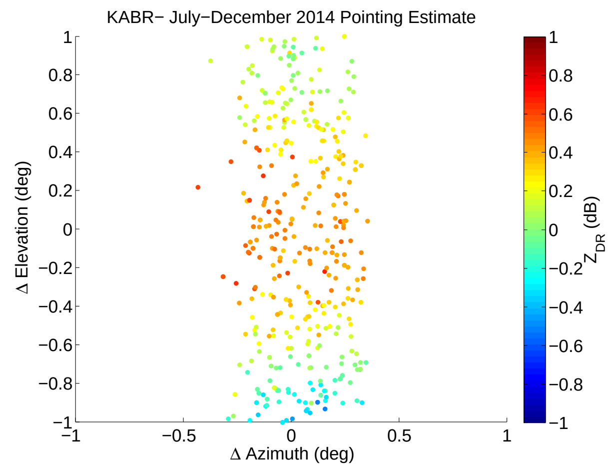

(b) An undesirable sun image collected at the KABR radar from July-December 2014. The colorfill indicates the median Z_{DR} in dB.

FIG. 4: Pre-Build 14 Pointing Estimates (a) compared with Build 14 Estimates (b). Δ values are represented as the difference between actual sun position and radar reported pointing.

$$P = Z(r) - 20\log_{10} r - 2ar - C_r \tag{A1}$$

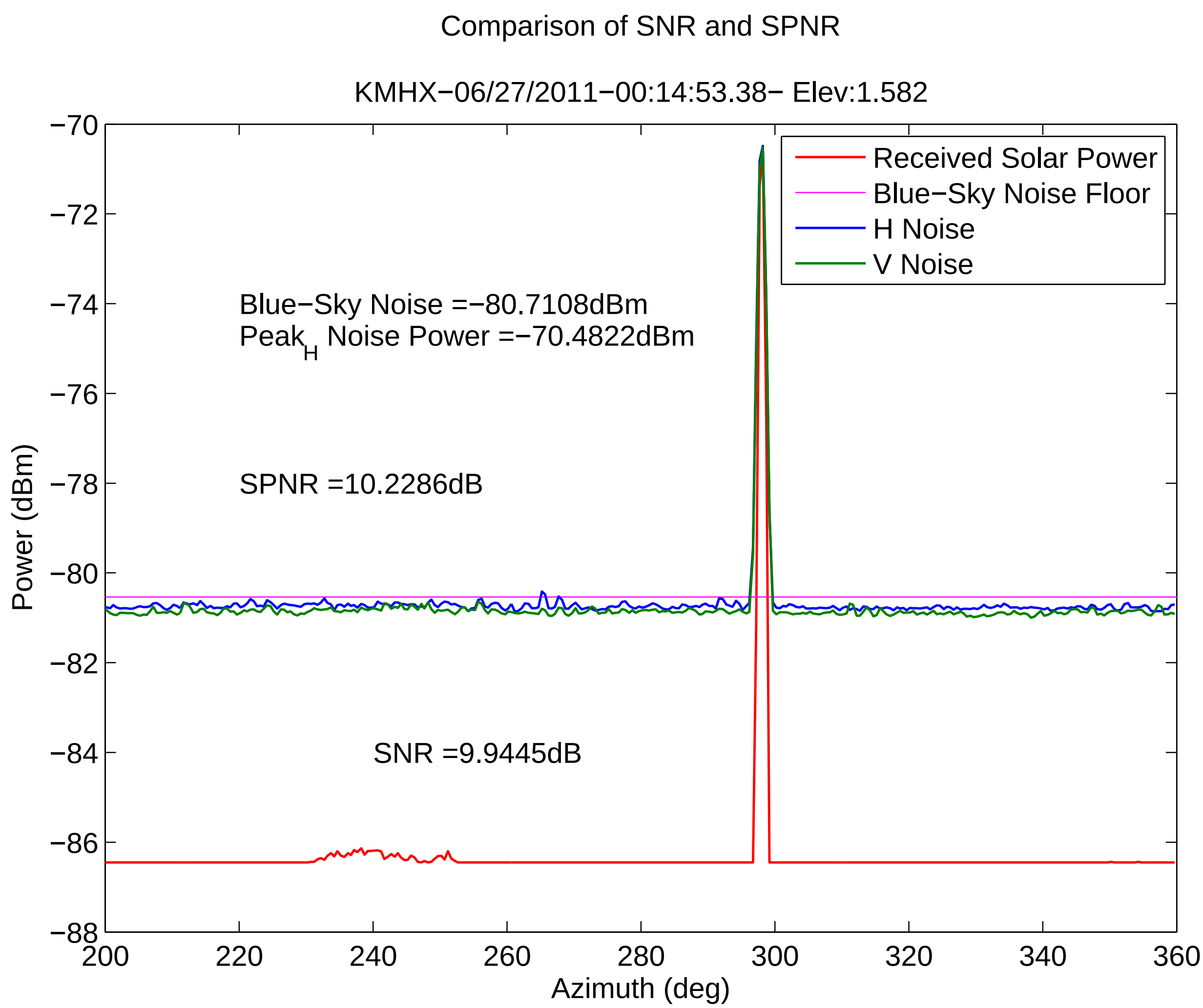

FIG. 5: Horizontal and Vertical Channel Noise overlayed with the Received Solar Power, observed at the KMHX radar.

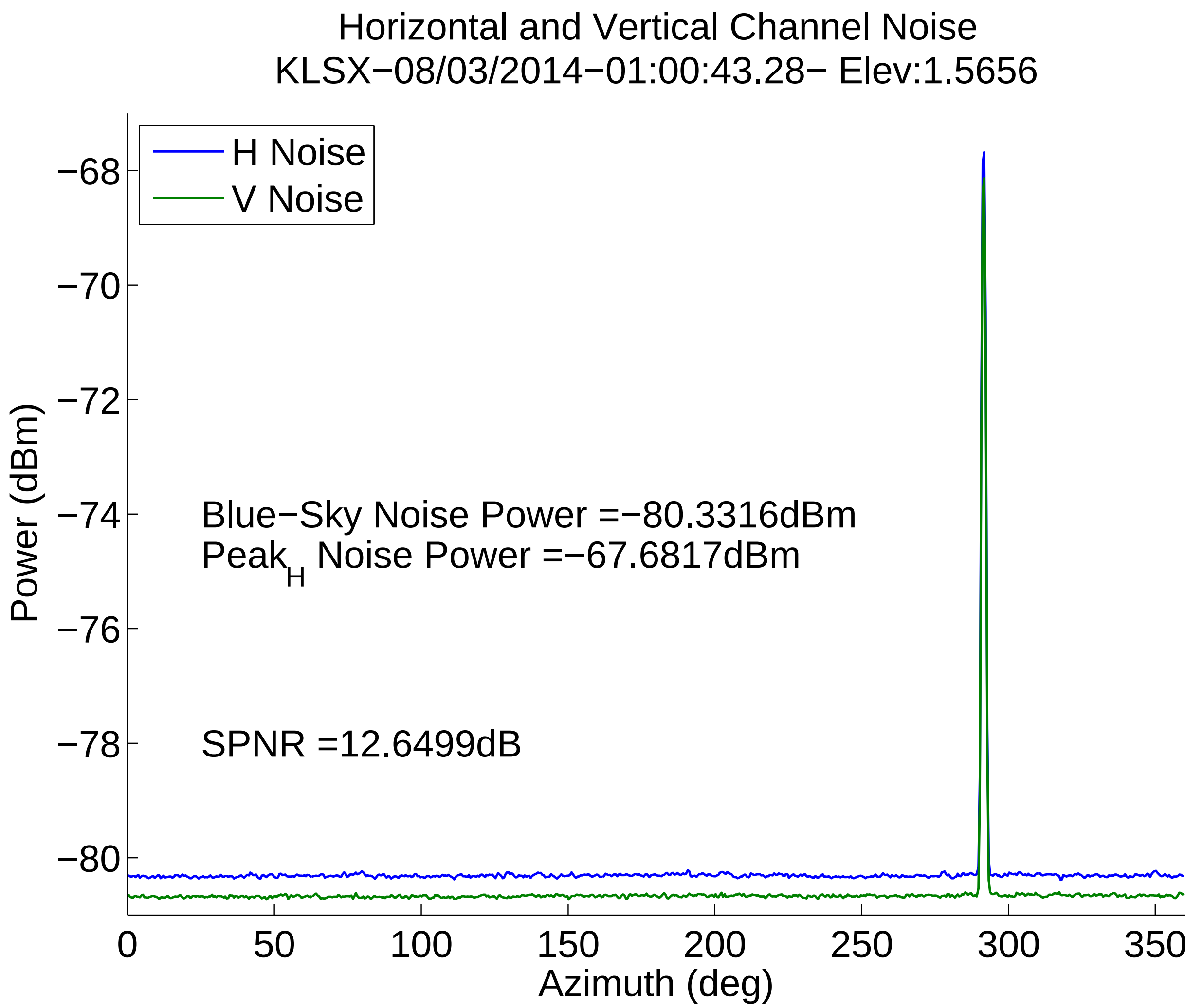

FIG. 6: Radial-by-Radial Noise output at the KLSX radar on 3 August 2014 demonstrating the signature of a strong sunspike.

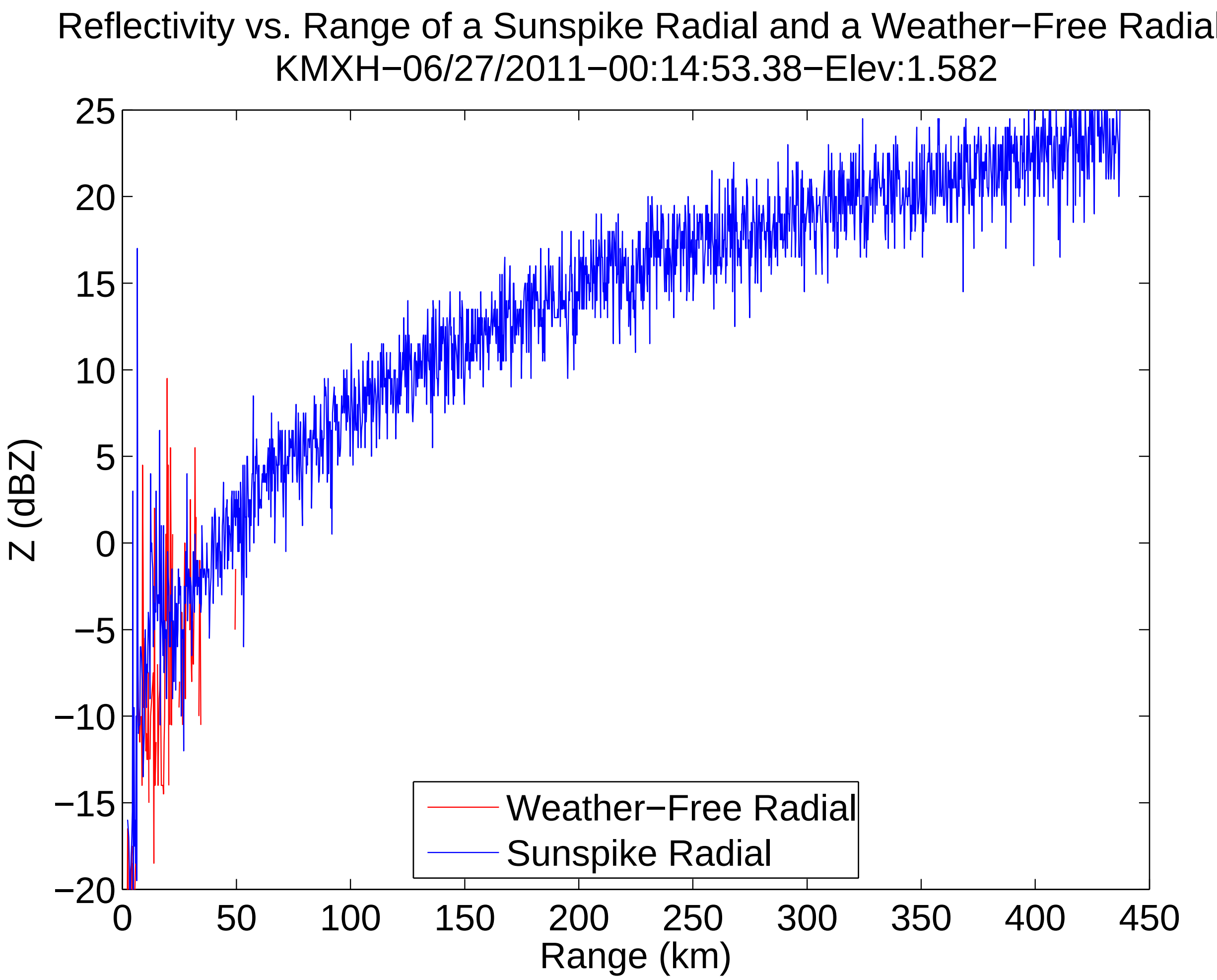

FIG. 7: Comparing the Reflectivity profiles of a sunspike radial and a weather-free radial, observed at the KMHX radar.

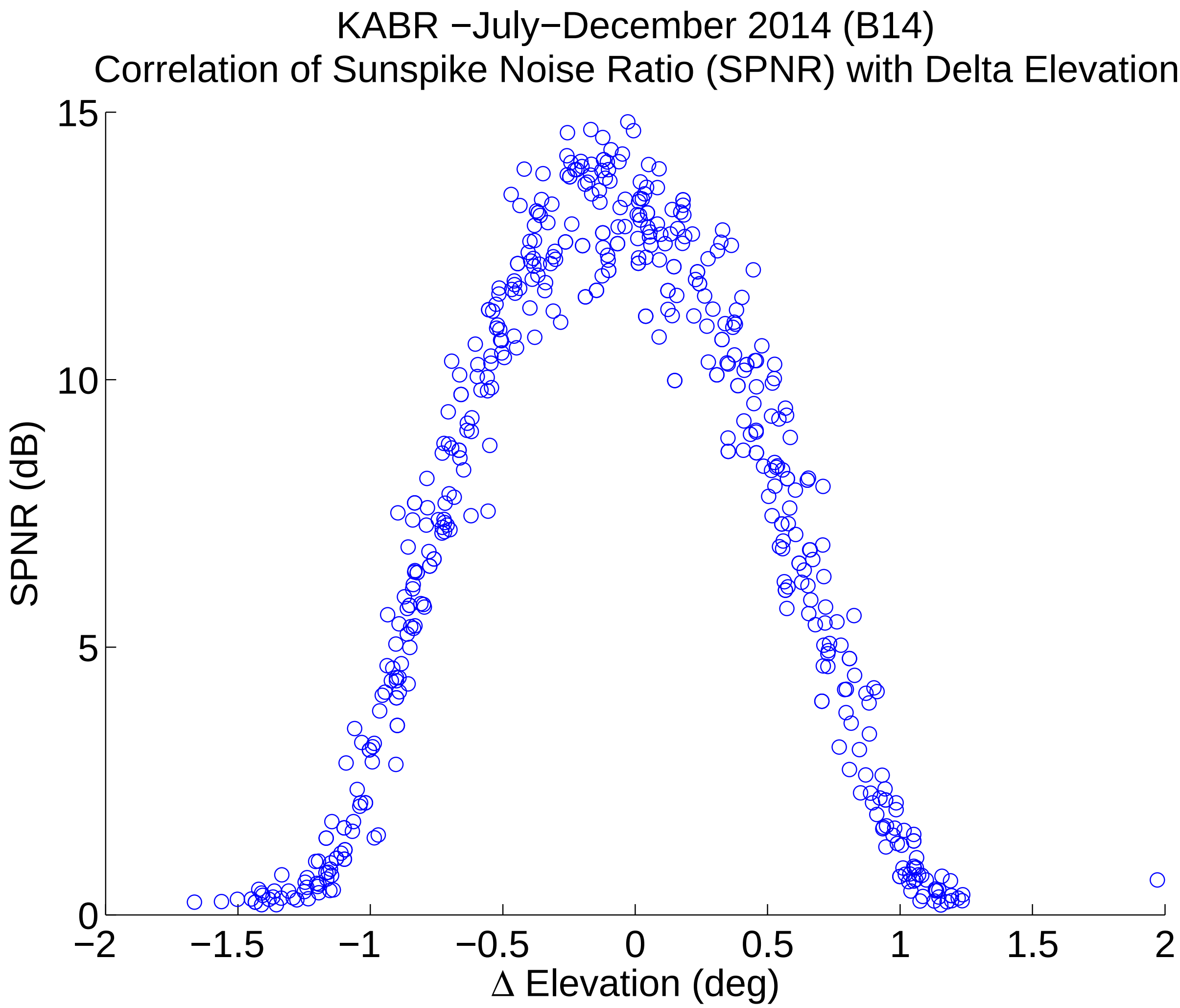

FIG. 8: Correlation between SPNR and Δ Elevation over July-December 2014, observed at the KABR radar. Δ values are represented as the difference between actual sun position and radar reported pointing.

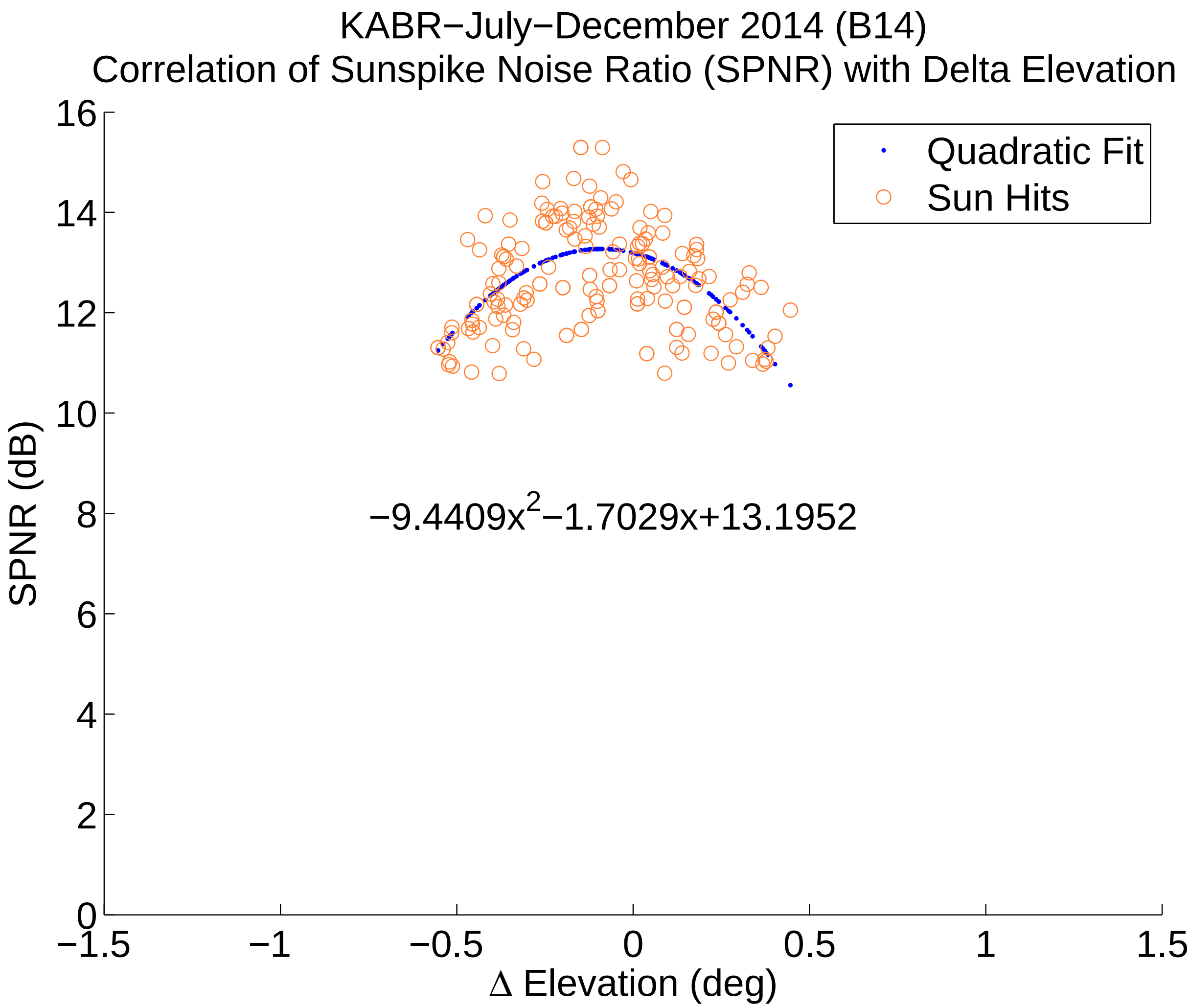

FIG. 9: Correlation between SPNR and Δ Elevation over July-December 2014 after including the SPNR threshold of $\geq$ 10dB, observed at the KABR radar. Δ values are represented as the difference between actual sun position and radar reported pointing.

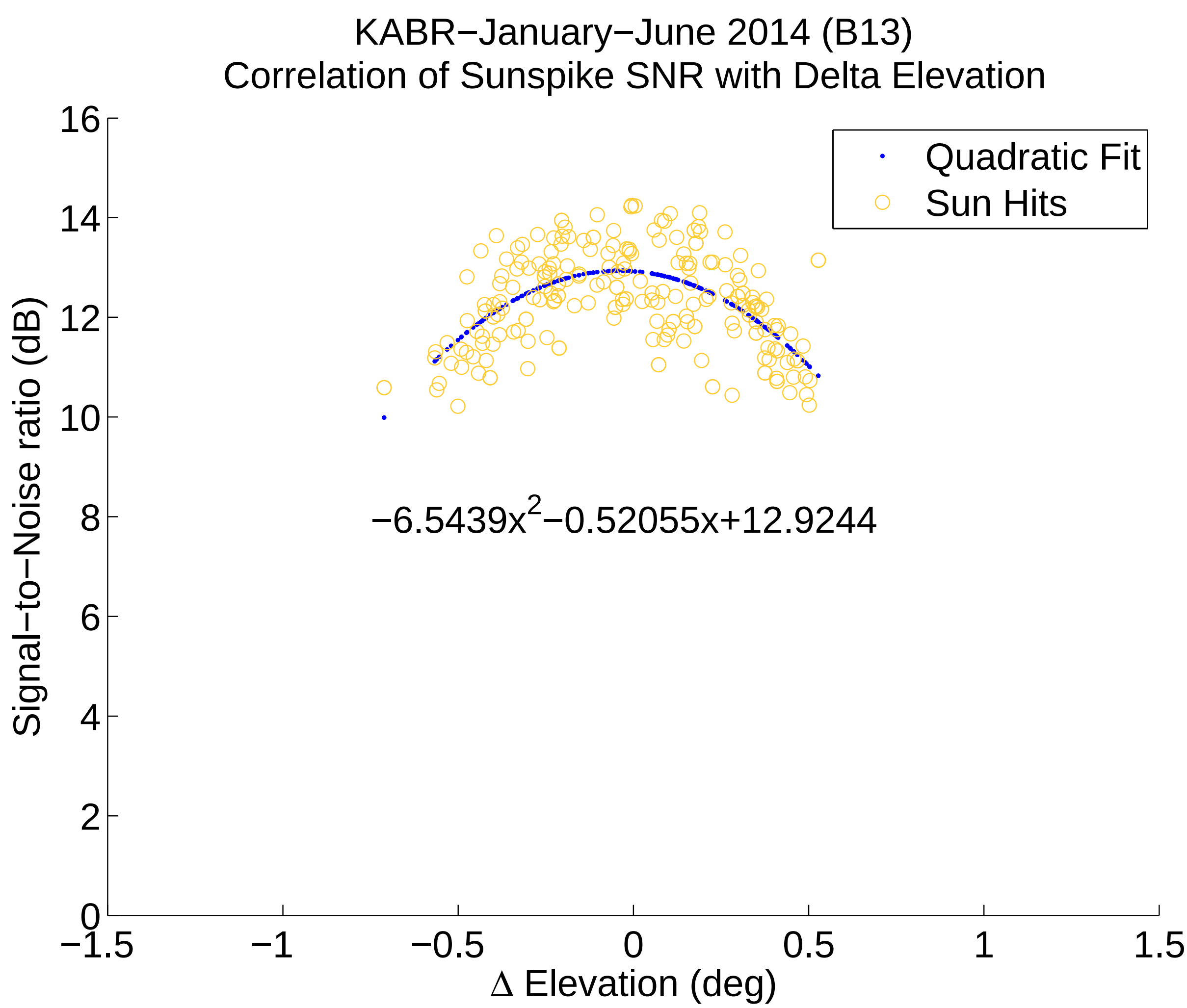

FIG. 10: Correlation between SNR and Δ Elevation over January-June 2014, observed at the KABR radar. Δ values are represented as the difference between actual sun position and radar reported pointing.

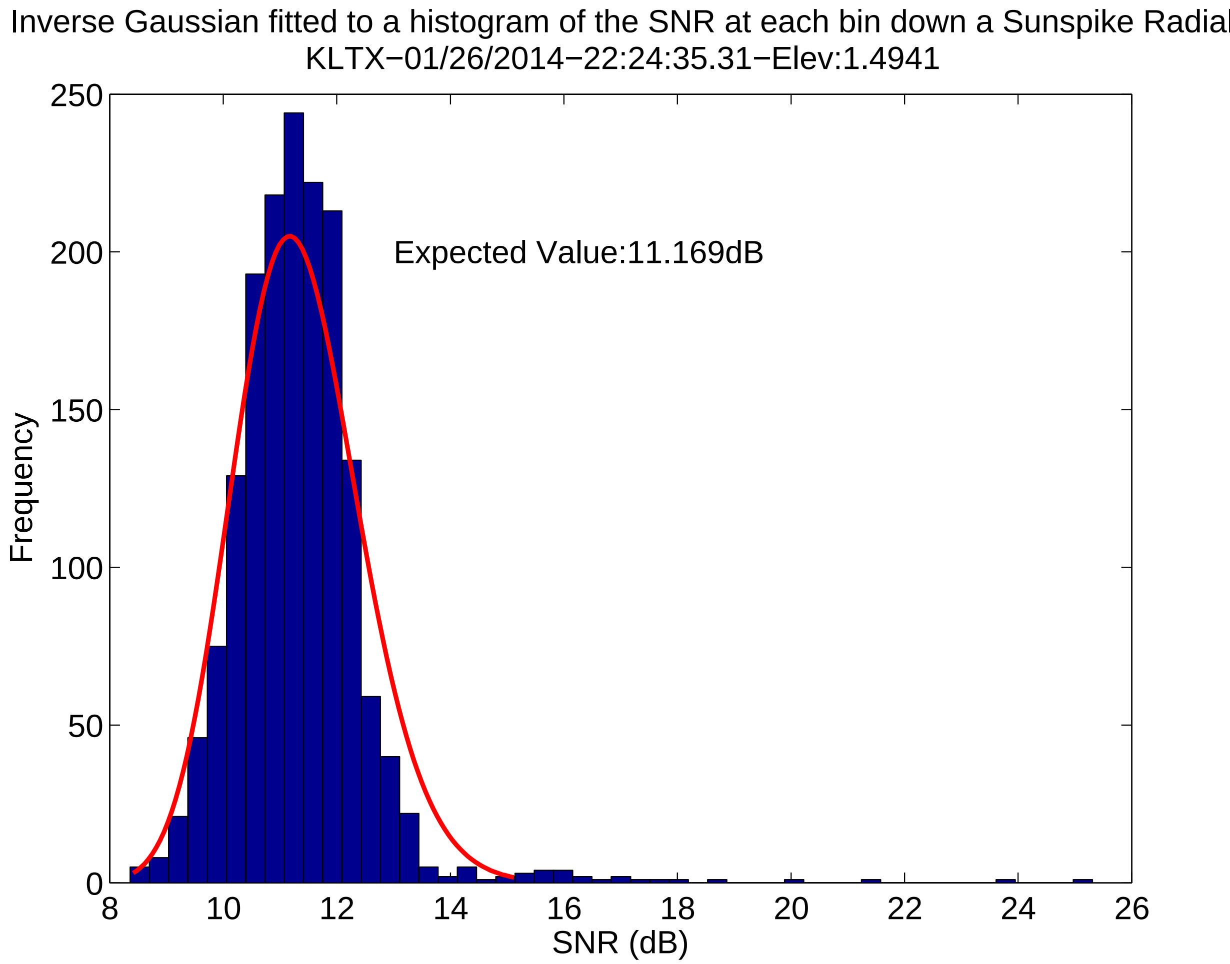

FIG. 11: A Histogram of SNR, calculated at each bin down a sunspike radial, with an Inverse Gaussian fit. Observed at the KLTX radar on 26 January 2014.

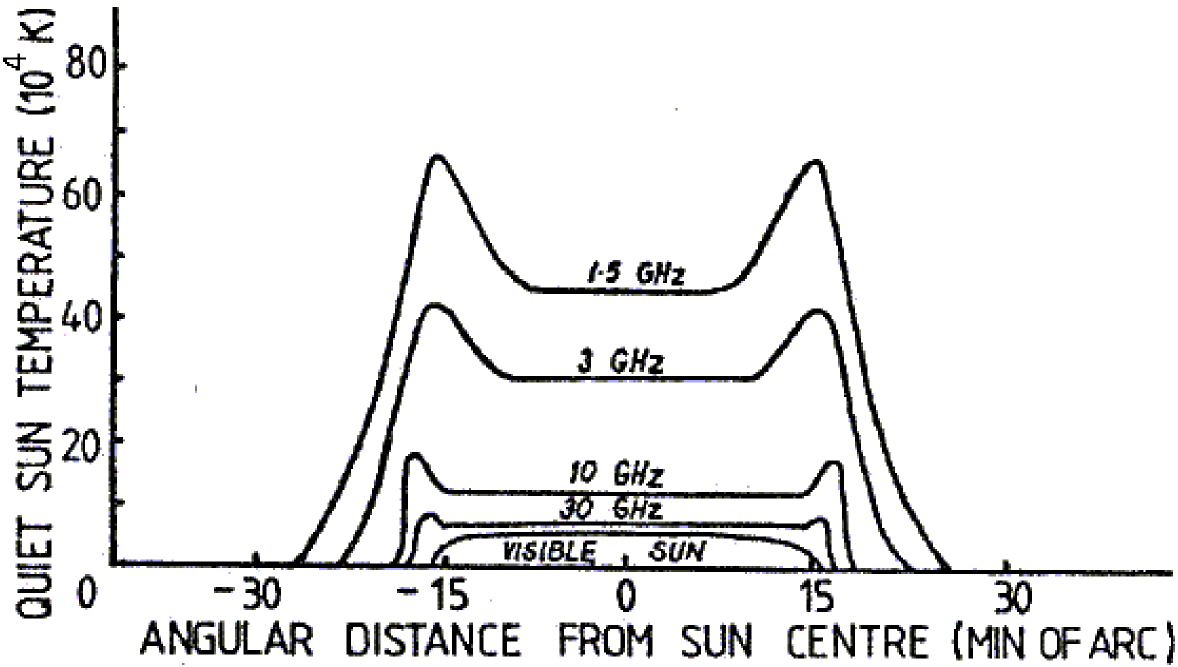

FIG. 12: Spatial Variation of Solar Microwave Emission after Kundu (1965)

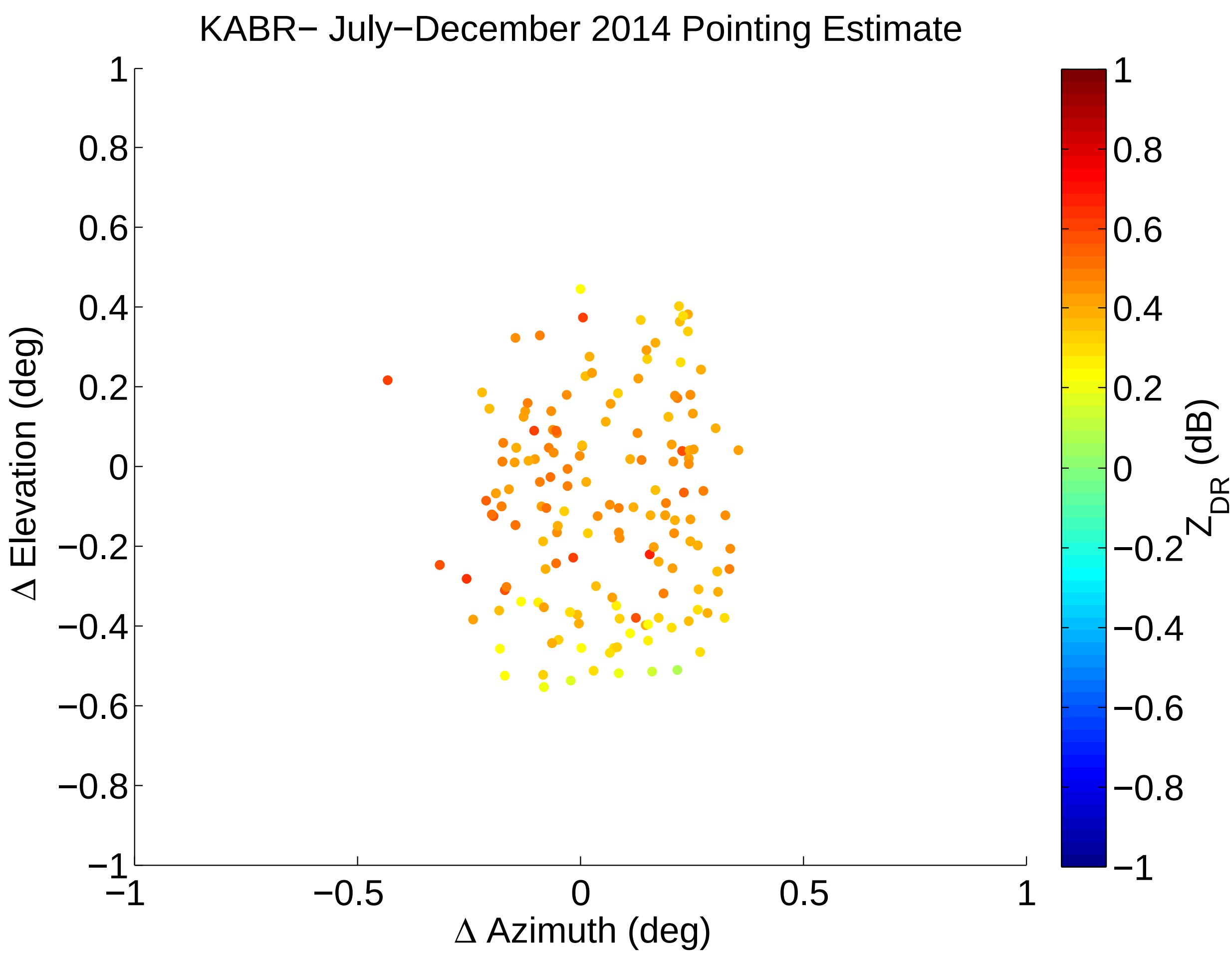

FIG. 13: Corrected Pointing Estimate collected at the KABR radar after including the SNPR threshold of $\geq$ 10dB.